MICROSTRUCTURES OF Ti-Al INTERMETALLIC COMPOUNDS IRRADIATED AT 673 K IN HFIR - Y. Miwa, T. Sawai (Japan Atomic Energy Research Institute), D. T. Hoelzer (Oak Ridge National Laboratory) and A. Hishinuma (JAERI)

OBJECTIVE

The objective of this work is to present recent TEM data of Ti-Al intermetallic compounds neutron irradiated at 673 K in High Flux Isotope Reactor.

SUMMARY

Four kinds of Ti-Al intermetallic compounds were irradiated at 673 K to the fluence of 5.16×10^{25} n/m^2 (E>1MeV) in HFIR. One consists of α_2-Ti_3Al single phase, and the others consist of α_2-Ti_3Al and γ-TiAl duplex phases. After irradiation, transmission electron microscopy was carried out. In both α_2-Ti_3Al and γ-TiAl phases of the specimens, loop-shaped and dot-like clusters were observed. However the nucleation behavior of cavities in α_2-Ti_3Al and γ-TiAl phases has been influenced by chemical compositions and fabrication processes.

PROGRESS AND STATUS

Introduction

Ti-Al intermetallic compounds offer advantages of large strength-to-weight ratio and high strength and good oxidation resistance at elevated temperature. In Ti-Al intermetallic compounds, α_2-Ti_3Al with the hexagonal ordered $D0_{19}$ structure and γ-TiAl with the tetragonal ordered $L1_0$ structure are promising candidates for nuclear apprication. Both Ti and Al are elements with low neutron-induced radioactivity and small cross sections of neutron absorption, compared with conventional austenitic stainless steels. In spite of the generation of a long-lived γ-emitter ^{26}Al from $^{27}Al(n,2n)^{26}Al$ reaction by 14 MeV neutron, the fast decay of radioactivity of Al to safe maintenance level within 2 weeks after reactor shutdown is attractive [1]. Therefore Ti-Al intermetallic compounds are attractive candidates for application in future fusion nuclear systems, as well as in fission nuclear systems.

Several papers have been published on the effect of electron irradiation [2], He^+ irradiation [3, 4, 5, 6] and neutron irradiation [7, 8] on Ti-Al intermetallic compounds. The ordered intermetallic compounds showed a superior resistance to void swelling under electron irradiation at 873 K [2], and ductilization after neutron irradiation at 873 K to 1×10^{24} n/m^2 (E>1MeV) [7]. On the other hand, they showed a poor resistance of He bubble nucleation in γ-TiAl after He^+ irradiation to 2.9 dpa at room temperature [6] and a significant ductility loss with neutron irradiation to the fluence level of 1.6×10^{26} n/m^2 at 376-873 K [8]. Little is known on the effects of irradiation, especially neutron-irradiation, on Ti-Al intermetallic compounds.

In this report, the microstructural observation of 4 kinds of Ti-Al intermetallic compounds irradiated at 673 K to the fast neutron fluence of 5.16×10^{25} n/m^2 (E>1MeV) are presented.

Experimental procedure

The materials used were 4 kinds of Ti-Al intermetallic compounds, and were produced by powder metallurgical processing. The powders for 3 kinds (K1, K2, K3) of intermetallic compounds were prepared by the mechanical alloying, and another powder for K4 was prepared by the plasma rotating electrode process (PREP). The nominal chemical compositions and notations are listed in Table 1. The conditions of powder metallurgical processes are also listed in Table 1. The nominal microstructures were an α_2-Ti_3Al single phase for K1, an α_2-Ti_3Al + γ-TiAl duplex phase for K2, a γ-TiAl single phase for K3, and an α_2-Ti_3Al + γ-TiAl duplex phase for K4, respectively. Hereafter, α_2 and γ denote α_2-Ti_3Al and γ-TiAl, respectively.

The powders used for K1, K2 and K3 had an average particle diameter of about 30 μm. The main impurities in those powders were Fe (50 ppm), C (70 ppm), H (120 ppm) and O (3200 ppm) in Ti, and Fe (1600 ppm) and Si (600 ppm) in Al, respectively. These powders were mixed in order to obtain the nominal compositions listed in Table 1. These mixed powders were then mechanically alloyed in an Ar gas atmosphere for 720 ks using a stainless ball mill. The mechanically alloyed powders were isostatically hot pressed in a pure titanium capsule in vacuum under 176.8 MPa at 1373 K for 10.8 ks to obtain high density compacts. In order to obtain higher strength and ductility, these compacts were annealed in vacuum at 1473 K for 36 ks.

The powder used for K4 was prepared from cast mother alloys by PREP, and had an average particle diameter of about 250 μm. A cylindrical compact, about 60 mm in diameter and about 100 mm in height, was made by hot isostatic pressing (HIP) under 176.8 MPa at 1323 K for 10.8 ks in a pure titanium capsule. This was followed by isothermal hot forging up to a reduction of 78% in height with a strain rate of $3.8 \times 10^{-4}\ s^{-1}$ at 1223 K in vacuum.

TEM disks, 3 mm in diameter and 0.25 mm in thickness, were prepared by wire cutting. These TEM disks were irradiated at about 673 K in a HFIR target position in the capsule of HFIR-MFE-JP20/position 9. The resulting thermal and fast neutron fluences, taking into account the specimen position in the reactor were $1.83 \times 10^{26}\ n/m^2$ (E<0.5 eV) and $5.16 \times 10^{25}\ n/m^2$ (E>1MeV), respectively [9]. The He production in Al was 6.42 appm [9]. The He production in Ti calculated by using the Japanese evaluated nuclear data library, JENDEL-3.2, was about 3.7 appm.

After irradiation, the disks were electrically thinned by a twin jet technique in a solution of 12.5 vol.% sulfuric acid and 87.5 vol.% methyl alcohol at 263 K with a constant current of about 150 mA and a varying voltage of 10~12 V. The TEM observation was carried out using a JEM 2000-FX microscope. The unirradiated disks were also observed using a Phillips CM12 equipped with an energy dispersive X-ray (EDX) analyzing system, VP9900.

Table 1 Nominal chemical compositions (atomic %) and heat treatment conditions

	Ti	Al	O	N	H	Powder	HIP	heat treatment
K1	65.78	31.49	1.49	0.17	1.08	MA	1373 K/10.8 ks/176.8 MPa	annealing/1473 K/ 36 ks
K2	52.53	45.90	1.26	0.12	0.19	MA	1373 K/10.8 ks/176.8 MPa	annealing/1473 K/ 36 ks
K3	49.30	48.11	2.31	0.19	0.09	MA	1373 K/10.8 ks/176.8 MPa	annealing/1473 K/ 36 ks
K4	52.41	46.87	0.63	0.06	0.03	PREP	1323 K/10.8 ks/176.8 MPa	hot forging/ 1223 K

MA: Mechanical alloying, PREP: Plasma rotating electrode processing

Results and discussion

Unirradiated Ti-Al intermetallic compounds

Figure 1 shows low-magnification microstructures of the unirradiated Ti-Al intermetallic compounds. In mechanically alloyed compounds (K1, K2 and K3), the grain size of K1 (fig. 1(a)) was the largest, and that of K3 (fig. 1(c)) was the smallest. The grain size of K4 (fig. 1(d)) which was made by PREP was larger than that of K1. The ASTM grain size numbers measured by lineal analysis were listed in table 2. The distribution of phases observed in the microstructures of fig. 1 is illustrated schematically in figure 2.

Table 2 ASTM grain size number before and after irradiation.

	before irradiation	After irradiation
K1	16.8	16.9
K2	17.5	17.8
K3	19.1	18.7
K4	16.1	No observation

K1 consisted of a duplex structure of matrix and island grains, as seen in figs. 1(a) and 2(a). The matrix was α_2 phase. The islands existed in matrix grains and along grain boundaries. In the islands, the concentration of Ti was higher than that in the matrix, and a higher number density of planar defects was observed. From diffraction pattern analyses, the island grains seemed to be also α_2 phase. The volume fractions of matrix and island grains were ~93% and ~7%, respectively (table 3). The diametral size distribution of matrix and island grains is shown in fig. 3(a). The grain size of the islands was smaller than the matrix and was generally smaller than 1.0 μm. However a large island grain about 2 μm in diameter was observed. The maximum diameter of matrix grains was about 4 μm. The average diameter of matrix and island grains were ~1.64 μm and ~0.53 μm (table 4), respectively. No impurities were detected in both the matrix and islands by EDX analysis. Dislocation lines were not observed in the matrix and islands, but twin boundaries were observed in both. Pores were observed in grains and especially on grain boundaries (fig. 4(a)). The pores on grain boundaries seemed to be larger than those in grains. The pores had a variety of shapes, so the shorter diameter was measured in each pore. The diametral size distribution of pores is shown in fig. 5(a). The size distribution had a peak at about 8 nm, and the maximum diameter was about 70 nm. The pores in islands were smaller than those in matrix, and average diameter in islands and matrix were 9.7 nm and 14.4 nm, respectively (table 5). The number density of pores in K1 was about $6 \times 10^{19}/m^3$ (table 6), and that in island seemed to be higher than that in matrix. In these pores, Ar was detected by EDX analysis.

K3 was designed to be a single phase, γ-TiAl, intermetallic compound. However K3 consisted of three phases of Al_2O_3, α_2 and γ. The volume fractions among Al_2O_3, α_2 and γ were 3~4%, ~10% and ~87%, respectively (table 3). In the other intermetallic compounds, there were no alumina grains. The diameter of most alumina grains ranged from 0.3 to 0.9 μm, but larger grains ranging to 2.8 μm in diameter also existed. The average diameter of alumina grains was ~0.63 μm. Impurities such as P, Ti, Cr, Fe, Ni and Ar were detected in alumina by EDX analysis. As seen in figs. 1(b) and

2(b), relatively larger γ grains and smaller α_2 grains were observed. Figure 3(b) shows the diametral size distribution of γ and α_2 grains. The average diameter of α_2 and γ grains were 0.46 μm and 0.83 μm, respectively (table 4). The diameter of α_2 grains was not larger than 1.0 μm, and that of γ grains was over 2 μm. From EDX analyses, impurities such as Fe, Cr and Ni were detected in γ phase, but not in α_2 phase. It appeared that these impurities came from the stainless balls during mechanical alloying processes. From the comparison of the presence of impurities between γ and α_2 phase in K1 and K2, it seemed to be more difficult to dissolve the impurities in α_2 phase than in γ phase. Twin boundaries were observed in γ grains, but only a few twin boundaries were observed in α_2 grains. There were pores in γ grains and especially on grain boundaries (fig. 4(b)). Pores were not typically observed in the α_2 grains. The diametral size distribution of the pores is shown in fig. 5(b). The size distribution has a peak at ~10 nm, and the maximum diameter was ~70 nm. The average diameter of the pores was ~13.0 nm (table 5). The distribution of pores which existed on γ-γ boundaries was similar to that in K1 which had only α_2-α_2 boundaries. The number density of pores in K3 was about 9×10^{19} /m^3 (table 6). In these pores, Ar was detected by EDX analysis.

K2 was designed to have a duplex microstructure consisting of the α_2 and γ phases in order to obtain better ductility. The analysis of K2 showed that it consisted of two phases. The volume fraction of α_2 and γ phases measured by areal analysis were ~22% and ~78%, respectively (table 3). A combination of relatively larger γ-TiAl grains and smaller α_2-Ti_3Al grains was observed, as seen in figs. 1(c) and 2(c). These microstructural characteristics were similar to that in K3 (figs. 1(b) and 2(b)). But the grain size in K2 is slightly larger than that in K3. The diametral size distribution of α_2 and γ grains is shown in fig. 3(c). The average diameter of α_2 grains in K2 was ~0.65 μm, and was larger than that in K3. The average diameter of γ grains in K2 was ~0.98 μm, and was similar to that in K3. The maximum diameter of γ grains in K2 was similar to that in K3, and was about 2 μm. Impurities such as Fe, Cr and Ni were detected in both α_2 and γ phases by EDX analysis. Though no impurities were detected in α_2 phase of K3 and also of K1, impurities were detected in α_2 phase of K2. The amount of impurities in α_2 phase of K2 is less than that in γ phase. Twin boundaries were observed in both α_2 and γ grains. Twin boundaries existed in α_2 grains of K2, but few twin boundaries existed in those of K3. Pores were observed in grains and especially on grain boundaries, as seen in fig. 4(c). The pores were not observed in α_2 grains, which was a similar result to K3. Therefore it is more difficult for pores to occur in α_2 phase than in γ phase. Figure 5(c) shows the diametral size distribution of pores in K2. The diametral size distribution has two peaks at ~4 nm and 10~12 nm, and the maximum was about 60 nm. The larger peak and maximum diameter in K2 were about the same as those in K3, and also about the same as those in K1. The average diameter and number density of pores in K2 were ~13.4 nm and ~6×10^{19} /m^3, respectively (table 5 and 6).

K4 consisted of a duplex microstructure of the α_2 and γ phases, as seen in figs. 1(d) and 2(d). The volume fraction of the α_2 and γ phases measured by areal analysis were ~11% and ~89%, respectively (table 3). Some α_2 grains were isolated within γ grains. These isolated α_2 grains sometimes crossed γ-TiAl grains, or arranged in parallel rows. The diametral size distribution of α_2 and γ grains is shown in fig. 3(d). The grain size of α_2 and γ grains in K4 was much larger than in both K2 and K3, which had similar duplex microstructures. The average diameter of α_2 and γ grains were ~1.07 μm and ~2.40 μm, respectively (table 4). No impurities were detected in the α and γ phases by EDX analyses. Dislocation lines and twin boundaries were observed in both α_2 and γ phases, as seen in fig. 4(d). The dislocation density in γ was 8~9×10^{13} /m^2. No pores were

observed in K4, which might have resulted from a fabrication process that used hot forging instead of mechanical alloying.

Table 3 The volume fraction of phases in Ti-Al intermetallic compounds (%)

	γ-TiAl	α_2-Ti_3Al	Al_2O_3
K1	-------	100 (Matrix: ~93, Island ~7)	-------
K2	~78	~22	-------
K3	~87	~10	3~4
K4	~89	~11	-------

Table 4 Average grain size of phases in Ti-Al intermetallic compounds (diameter, μm)

	γ-TiAl	α_2-Ti_3Al
K1	-------	matrix : 1.64, island : 0.53
K2	0.98	0.65
K3	0.83	0.46
K4	2.40	1.07

Table 5 Average diameter of pores in Ti-Al intermetallic compounds (nm)

	γ-TiAl	α_2-Ti_3Al
K1	-------	matrix : 14.4, island : 9.7
K2	13.4	
K3	13.0	
K4	No	

Table 6 The number densities of pores in Ti-Al intermetallic compounds (m^{-3})

K1	~ $6x10^{19}$
K2	~ $6x10^{19}$
K3	~ $9x10^{19}$
K4	No

Irradiated Ti-Al intermetallic compounds

After irradiation, the TEM specimens were stored for about 5 years to decay the radioactive isotope. The dose rates of TEM specimens were ~9.8 mR/h at 1 cm in K1, ~53 mR/h at 1 cm in K2, ~150 mR/h at 2.54 cm in K3 and ~3.7 mR/h at 1 cm in K4, respectively. As seen in the nominal chemical compositions in table 1, the amount of impurities such as Fe, Cr and Ni were not

measured, but these impurities were detected by EDX analysis. By assuming that the ionizing radiations mainly come from these impurities, the amount of these impurities in K1 was the lowest among mechanically alloyed specimens of K1, k2 and K3. The amounts of these impurities in K2 and K3 were about five times and over fifteen times higher than in K1, respectively. This estimation about the amounts of these impurities corresponded roughly to the results of EDX analysis.

The ASTM grain size number of the Ti-Al intermetallic compounds after irradiation were similar to those before irradiation. Those numbers are listed in table 2.

Figures 6(a) and (b) show cavities observed in both the matrix and island grains of the irradiated K1, respectively. The faceted cavities occurred in both matrix and islands after irradiation. The cavities in the matrix occurred preferentially around pores within the range of about 75 nm from the surface of the pores (fig. 6(a)). Some small cavities also occurred far from pores. The distribution of cavities in the matrix was not uniform. In the island grains where a high density of planar defects was observed before irradiation, the cavities were smaller than in matrix (fig. 6(b)). The number density of cavities in the islands was much higher than that in matrix. In the island, the cavities seemed to be arranged in rows, and few cavities were on the planar defects. On the grain boundaries between the matrix and island grains or between matrix grains, few cavities were observed. The diametral size distributions of cavities in the matrix and island grains are shown in figs. 6(c) and (d), respectively. The size of cavities in both matrix and island grains was much smaller than that of pores. The average diameter of cavities in the matrix and island grains was ~5.6 nm and ~3.4 nm, respectively (table 7). The maximum diameter in the matrix was ~10 nm, and was similar to that in the islands. The number densities of cavities in the matrix and island grains were ~4×10^{20} /m^3 and 2×10^{22} /m^3, respectively (table 8). Loop-shaped and dot-like defects were observed in both matrix and island grains, as seen in figs. 7(a) and (b). In the matrix, dislocation loops about 20 nm in diameter were observed. Some of these dislocation loops seemed to be tangled. In islands, smaller dislocation loops about 5 nm in diameter were observed. It seemed that the dislocation loops in the matrix were larger than those in the islands, and that the number density of dislocation loops in the islands was higher than that in the matrix. In both the matrix and island grains, these dislocation loops occurred near the grain boundaries and near cavities or pores. In the island grains, the planar defects which existed before irradiation remained after irradiation.

In irradiated K3, small cavities occurred only in the γ phase. Figures 8(a) and (b) show that the faceted cavities occurred uniformly in γ grains. As seen in fig. 8(a), there were cavity free zones around γ-γ grain boundaries, and the width of the cavity free zones was about 100 nm. However, there was a γ-γ grain boundary where many cavities occurred. There were no cavities around pores in γ grains, which was different from the cavity nucleation behavior in α_2 phase of K1. In the α_2 grains of K3, no cavities were observed after irradiation, though many cavities occurred in α_2 grains of K1. The diametral size distribution of cavities in γ phase is shown in fig. 8(c). This size distribution looked like a bi-modal distribution, and has two peaks at ~2 nm and ~10 nm. This distribution did not include the pores located on grain boundaries. The larger peak in the diametral size distribution of cavities was similar to the peak for pores. The maximum diameter was ~ 20 nm, which was larger than that in K1. The average diameter and number density of cavities in γ phase were ~9.4 nm and ~2×10^{21} /m^3, respectively (table 7 and 8). Loop shaped clusters and dot-like defects formed in both γ and α_2 phases after irradiation. Figures 9(a) and (b) show the dislocation

loops in γ and α_2 grains, respectively. The dislocation loops in γ grains were smaller than those in α_2 grains, and the diameter was about 5 nm. The loop diameter in α_2 grains was about 15 nm. In the γ grains, the number density of dislocation loops near grain boundaries seemed to be lower than that in grain interiors. However the loop density near twin boundaries in the grain was not different from that in grain interiors, and defects existed on the twin boundaries. The dislocation loops also existed near both cavities and pores.

Figures 10(a) and (b) show the cavities that were observed in both the α_2 and γ phases in irradiated K2. As seen in fig. 10(a), small cavities appeared in some γ grains, but not in all the γ grains. There were no cavities around pores in γ grains, which was similar to K3. There were no cavities on γ-γ grain boundaries, but there were some cavities on twin boundaries in γ grains. On the other hand, a higher density of small cavities occurred in α_2 grains (fig. 10(b)). These cavities were faceted. The cavities appeared around pores in the range of about 75 nm from surface of pore, which was similar to the cavity nucleation behavior in K1. The cavities also formed on α_2-γ grain boundaries (fig. 10(a)). The diametral size distributions of cavities in γ and α_2 grains are shown in figs. 10(c) and (d), respectively. The size distribution of cavities including pores in γ phase shows a bi-modal distribution (fig. 10(c)). From a comparison of the diametral size distributions of pores or cavities in γ phase before (fig. 5(c)) and after irradiation (fig. 10(c)), it appeared that the fraction of cavities that were 4~6 nm in diameter increased and the peak for larger cavities group shifted from 10~12 nm before irradiation to ~20 nm after irradiation. This suggested that irradiation might cause nucleation of small cavities and growth of the pores. As seen in fig. 10(d), the diametral size distribution of cavities in α_2 phase was similar to that in α_2 phase (matrix) of K1. The average diameter of cavities in α_2 and γ grains were ~5.7 nm and ~17.5 nm, respectively (table 7). The number densities of cavities in α_2 and γ grains were ~1×10^{21} /m^3 and ~4×10^{19} /m^3, respectively (table 8).There were loop-shaped and dot-like defects in both α_2 and γ phases after irradiation. Figures 11(a) and (b) show the dislocation loops in γ and α_2 grains, respectively. The diameter of dislocation loops in γ grains was similar to or slightly larger than that in α_2 grains. These dislocation loops were about 10 nm in diameter. The number density of dislocation loops in α_2 grains seemed to be higher than that in γ grains. These defects existed near grain boundaries and cavities.

In irradiated K4, TEM specimen did not electropolish uniformly which resulted in limited thin regions of the foil. As a result, only two γ grains were observed. In these γ grains, small cavities occurred after irradiation, as seen in fig. 12(a). These faceted cavities formed along the dislocation lines which existed before irradiation. There were some cavities on twin boundaries in the γ grain, but no cavities on grain boundaries. Figure 12(b) shows the diametral size distribution of cavities in γ grains. A bi-modal distribution was observed. The critical diameter of smaller cavities was ~2 nm. The average diameter and number density of cavities in γ grains were ~5.6 nm and ~8×10^{20} /m^3, respectively (table 7 and 8). Large stacking fault dislocation loops that were about 50 nm in diameter formed in γ grains. Figure 13(a) and (b) show the dislocation loops the γ grain. These dislocation loops were much larger than those in γ grains of K2 or K3. These loops formed near the dislocation lines that existed before irradiation, and also formed preferentially near grain boundaries. The distribution was not uniform. The number density of dislocation loops was much lower than that in γ-TiAl grains of K2 or K3.

Table 7 Average diameter of cavities in phases (nm)

	γ-TiAl	α_2-Ti_3Al
K1	-------	matrix : 5.9, island : 3.4
K2	17.5	5.7
K3	9.4	No
K4	5.6	xxxxxxxx

xxxxxxxx : TEM observations were not carried out

Table 8 Number densities of cavities in phases (m^{-3})

	γ-TiAl	α_2-Ti_3Al
K1	-------	matrix : ~$4x10^{20}$, island : $2x10^{22}$
K2	$4x10^{19}$	$1x10^{21}$
K3	$2x10^{21}$	No
K4	~$8x10^{20}$	xxxxxxxxx

xxxxxxxx : TEM observations were not carried out

Cavity nucleation in α_2-Ti_3Al and γ-TiAl phase

Cavities formed in both α_2 and γ phases during neutron irradiation at 673 K, though there were some exceptions in K2 and K3. This irradiation temperature corresponded to 0.27 T_m (T_m: melting point) for γ and 0.34 T_m for α_2, respectively. The size distributions of cavities looked like bi-modal distributions. The relatively larger cavities were faceted. This suggests that the larger cavities might be voids. It is well-known that voids form during irradiation in the temperature range from 0.3 to 0.55 T_m in metals. It was expected, therefore, that the Ti-Al ordered intermetallic compounds also experienced void swelling in this temperature range.

In the α_2 phase of K1, K2 and K3, cavities formed in K1 (both the matrix and islands) and in K2, but not in K3. In K1 and K2, the cavities formed preferentially around pores. These pores existed prior to irradiation, and contained Ar gas. The range where cavities existed from the surface of pores was about 75 nm. It is suggested that Ar is recoiled from the pore by the elastic collision with neutrons, which makes an atomic displacement, and assists the nucleation of gas bubble. The maximun recoil energy of Ar with 1 MeV neutron by the elastic scattering was about 96 keV. The range of these energetic Ar ions in α_2 phase was calculated using TRIM 85 with the displacement energy of 25 eV for both Ti and Al, and was about 73 nm. This calculated range corresponded well to the measured range of cavities from the pores surface. Therefore the cavities around pores might be Ar gas bubble, and Ar gas might assist the nucleation of cavities. In K3, however, cavities were not observed both in α_2 grains and around pores. The Ar gas was also detected in pores of K3. This means that the presence of Ar gas and other gas might be the key factor for the formation of cavities in the α_2 phase. In addition to Ar gas, helium was also generated from nuclear reactions of Al and Ti. The calculated He concentration in α_2-Ti_3Al was about 4.4 appm. However although helium was produced in K3, cavities were not observed. Therefore this amount of helium might

not have an influence on the cavity nucleation, or might be less effective than Ar. Oxygen is also present in these compounds. K3 contained twice the amount of oxygen compared to K1 or K2. However alumina was observed only in K3, and the volume fraction of alumina was about 3%. From the estimation of the amount of oxygen in alumina, almost all oxygen sis assosiated with alumina. Therefore K1 and K2 dissolved the oxygen, but K3 dissolved much less oxygen. This suggested that the oxygen had an influence on the cavity nucleation in the α_2 phase. Other impurities such as Fe, Cr and Ni were detected only in K2 but not in K1 and K3, which did not correspond to the nucleation behavior of cavities among them.

In the γ phase, the cavities were observed in every specimen, except for K1. However there were differences in the nucleation behavior of cavities among K2, K3 and K4. In K2, the number density of cavities was much lower than in K3 and K4. In K3, the number density of cavities was the largest, and cavities formed uniformly in γ grains. In K4, cavities occurred along dislocation lines which existed before irradiation. The size distribution of cavities in K3 and K4 showed bi-modal distributions. In all the γ grains investigated, there were no cavities near pores. Therefore the Ar gas in pores was not effective to form cavities in γ phase, which was different from the effect of Ar in α_2 phase. The calculated concentration of He gas which was generated from nuclear reaction of Ti and Al was about 5 appm. This amount is similar among K2, K3 and K4. Such an amount of He gas had little influence on the nucleation behavior of cavities in γ phase. Oxygen was also contained in these materials. Though the content of oxygen was highest in K3, almost all the oxygen was tied up with alumina, as discussed above. The amount of free oxygen in K3 seemed to be very low. The amount of oxygen in K2 was higher than in K4. The number density of cavities was the largest in K3, and the smallest in K2. Therefore the tendency of oxygen gas affecting the cavity nucleation in γ phase was opposite in α_2 phase. Nakata et. al. reported a similar effect of gas atoms on cavity nucleation behavior in He^+ ion irradiation experiment [3, 4]. In front of the calculated projected range of He ions, where the He concentration was very low, the number density of cavities in γ phase was larger than that in α_2 phase [3]. In the calculated projected range of He ion, where the He concentration was high, the number density of cavities in α_2 phase was larger than that in γ phase [4]. Therefore the effect of gas atoms on the cavity nucleation behavior might be different between γ and α_2 phases. Other impurities such as Fe, Cr and Ni were detected in K2 and K3 but not in K4. This did not correspond to the cavity nucleation behavior among them.

Reference

[1] T. Noda, F. Abe, H. Araki and M. Okada, J. Nucl. Mater. 155-157 (1988) 581-584.
[2] A. Hishinuma, K. Nakata, K. Fukai, K. Ameyama and M. Tokizane, J. Nucl. Mater. 199 (1993) 167-171.
[3] K. Nakata, K. Fukai, A. Hishinuma, K. Ameyama and M. Tokizane, J. Nucl. Mater. 202 (1993) 39-46.
[4] K. Nakata, K. Fukai, A. Hishinuma and K. Ameyama, J. Nucl. Mater. 240 (1997) 221-228.
[5] O. Okada, K. Nakata, K. Fukai, A. Hishinuma and K. Ameyama, J. Nucl. Mater. 258-263 (1998) 1750-1755.
[6] M. Song, K. Furuya, T. Tanabe and T. Noda, J. Nucl. Mater. 271&272 (1999) 200-204.
[7] A. Hishinuma, J. Nucl. Mater. 239 (1996) 267-272.
[8] A. Kohyama. T. Yamada, M. Ogawa, H. Matsui and M. Narui, Proc. of 2nd Japan/China Sym. on Materials for Advanced Energy Systems and Fission and Fusion Engineering (The University of

Tokyo, Japan, 1994) p.472.
[9] L. R. Greenwood and C. A. Baldwin, Fusion Reactor Materials Semiannual Progress Report, DOE/ER-313/23, p.305 (1997)

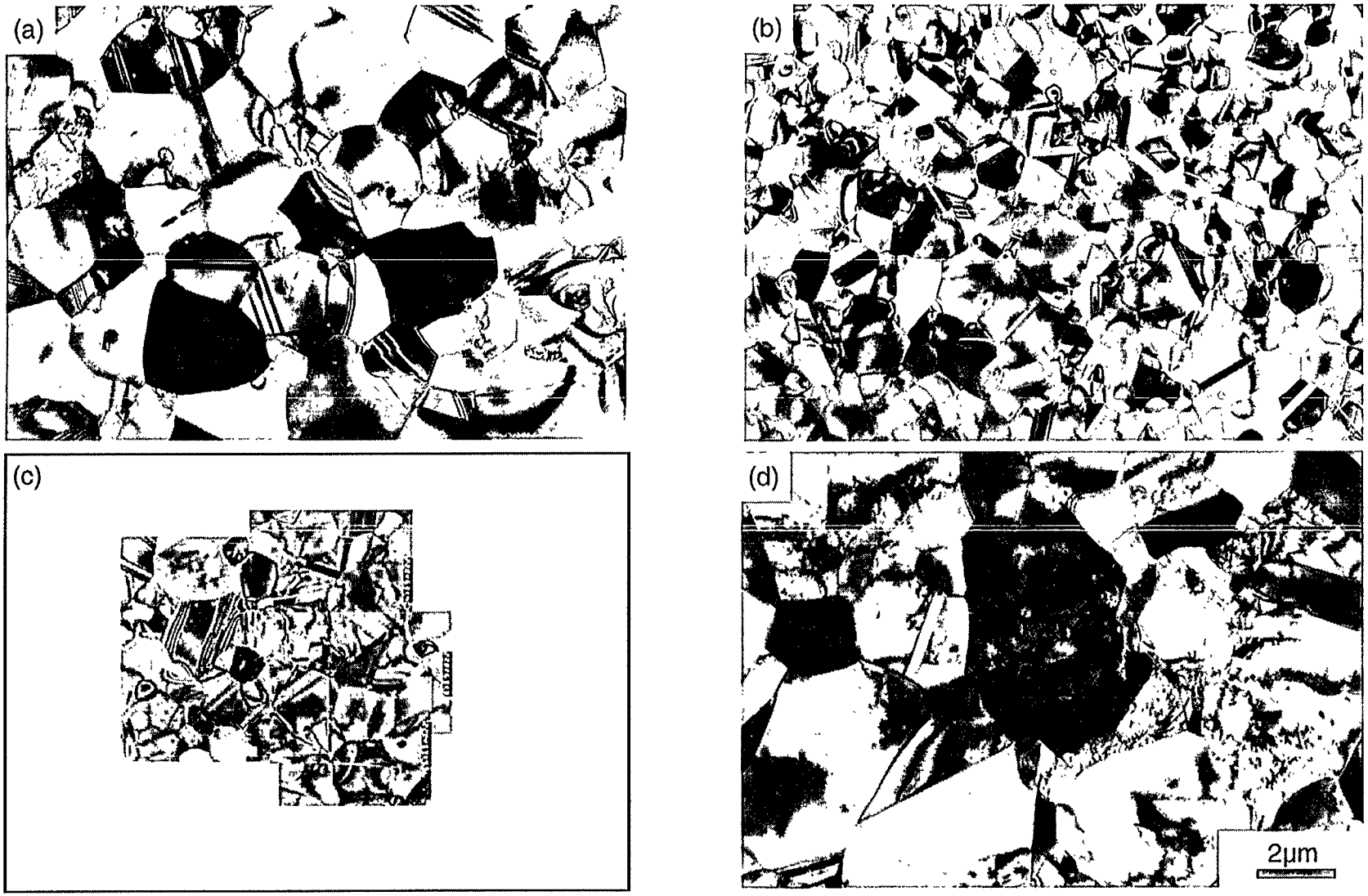

Figure 1 Low magnified TEM images of unirradiated Ti-Al intermetalic compounds.
(a) K1: α_2-Ti_3Al, (b) K3: γ-TiAl/α_2-Ti_3Al/Al_2O_3, (c) K2: γ-TiAl/α_2-Ti_3Al, (d) K4: γ-TiAl/α_2-Ti_3Al. K1, K2 and K3 were made by the mechanical alloying, and K4 was made by the plasma rotating electrode process.

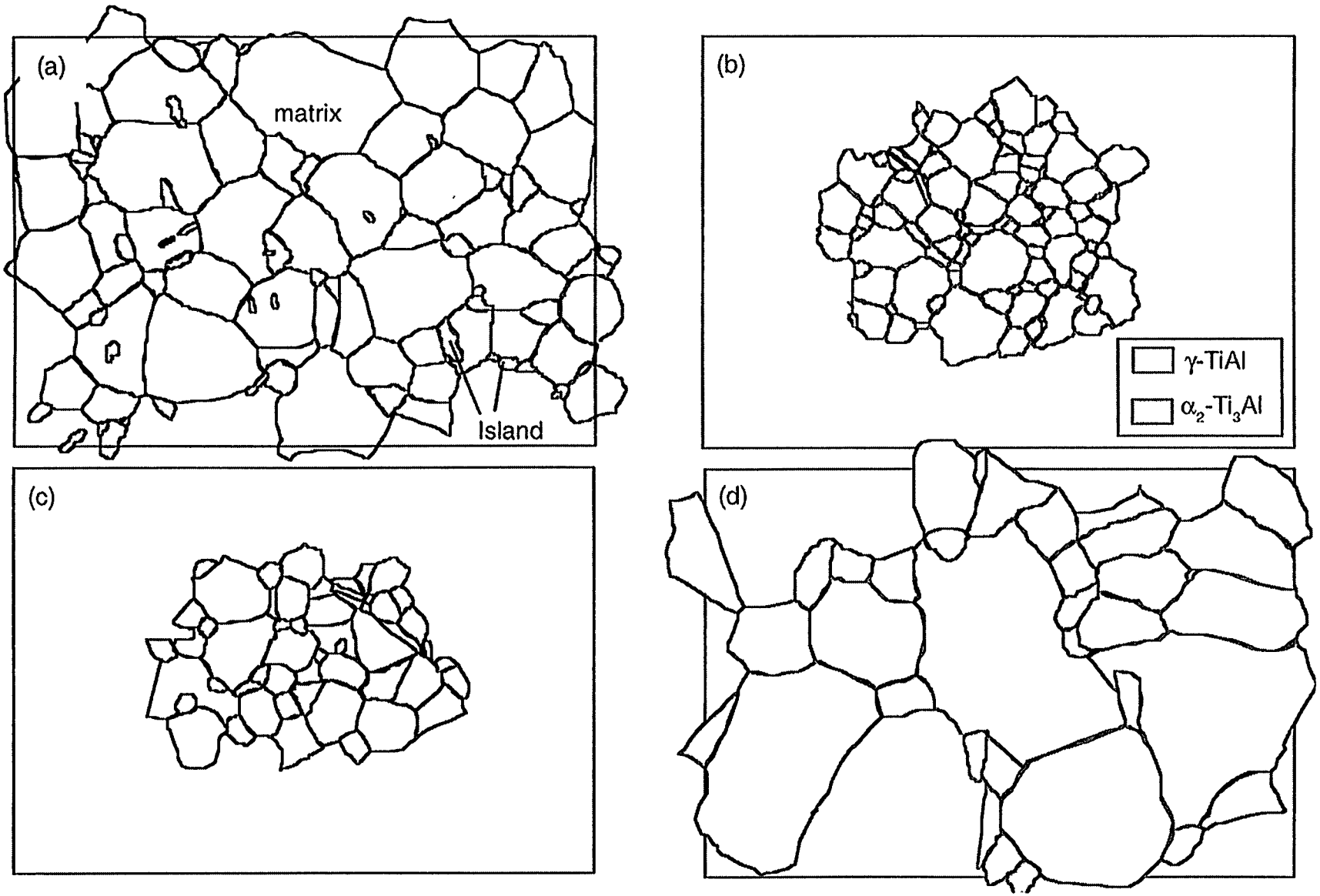

Figure 2 Schimatical illustrations of phase distribution of microstructures observed in figure 1.
(a) Duplex structure of matrix and island grains of α_2-Ti_3Al in K1; (b), (c) and (d) Distributions of γ-TiAl and α_2-Ti_3Al grains in K3 , K2 and K4, respectively.

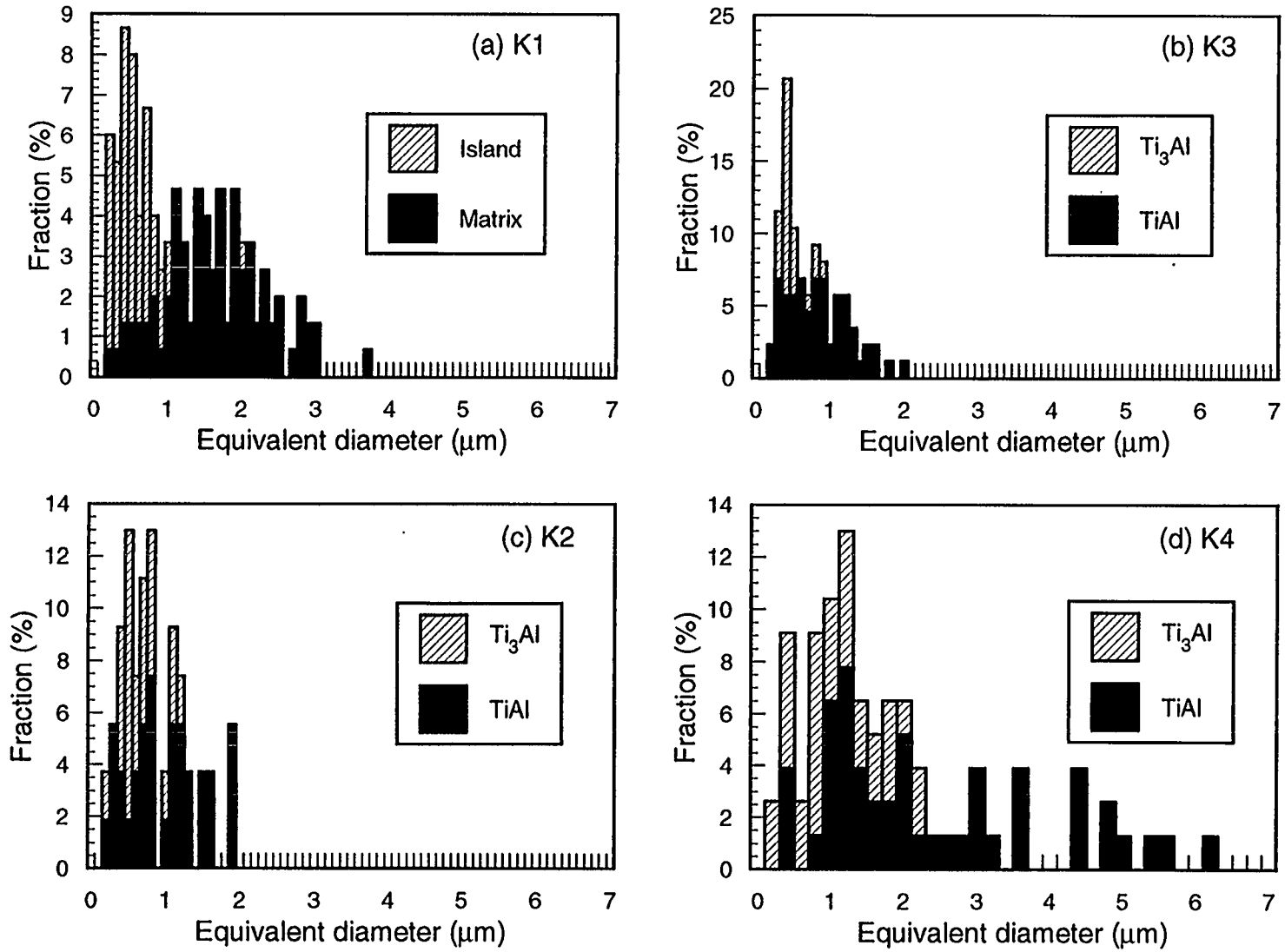

Figure 3 diametral size distributions of grains in unirradiated (a) K1, (b) K3, (c) K2 and (d) K4.

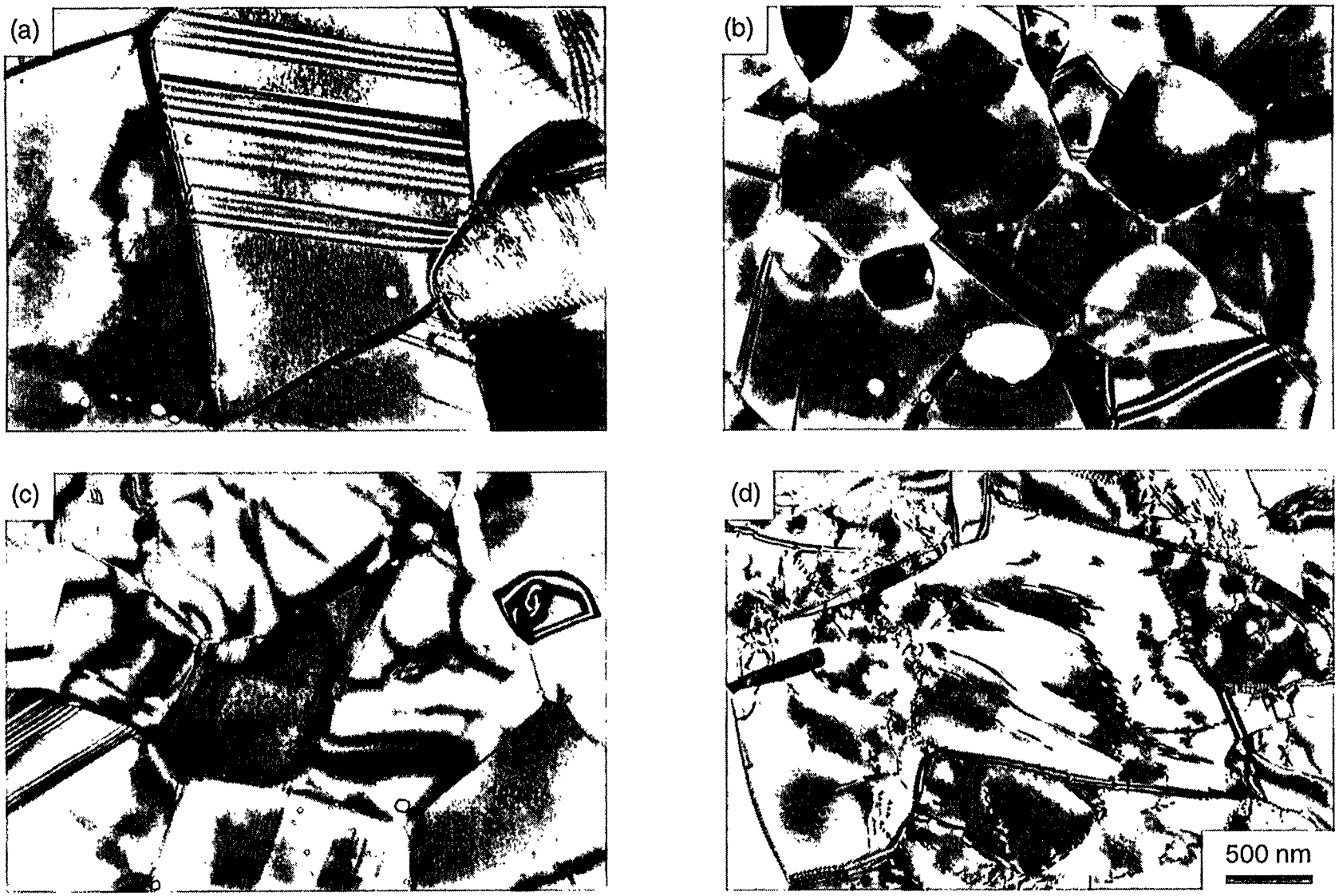

Figure 4 Microstructures of unirradiated (a) K1, (b) K3, (c) K2 and (d) K4. In mechanically alloyed K1, K3 and K2, pores were observed especially on grain boundaries.

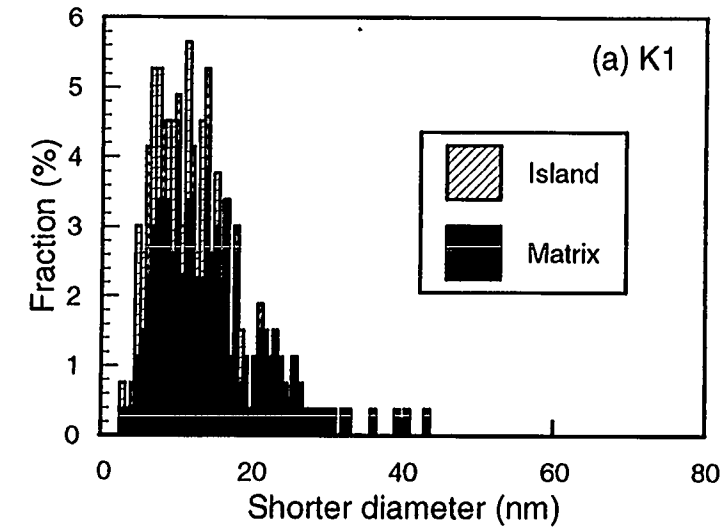

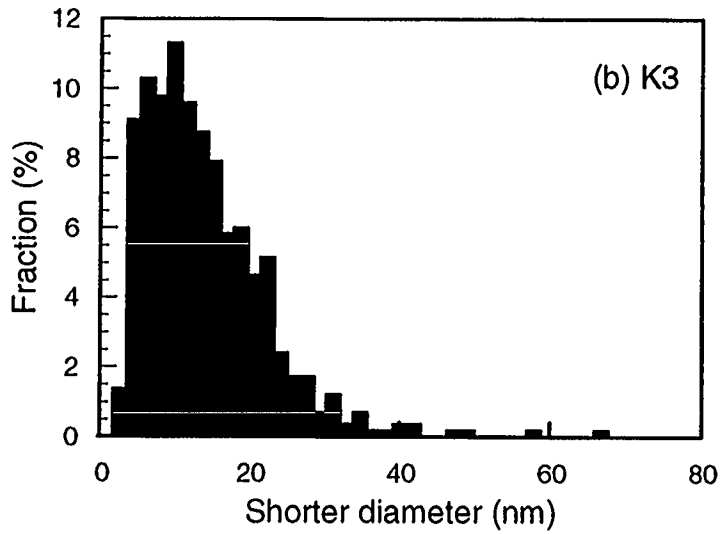

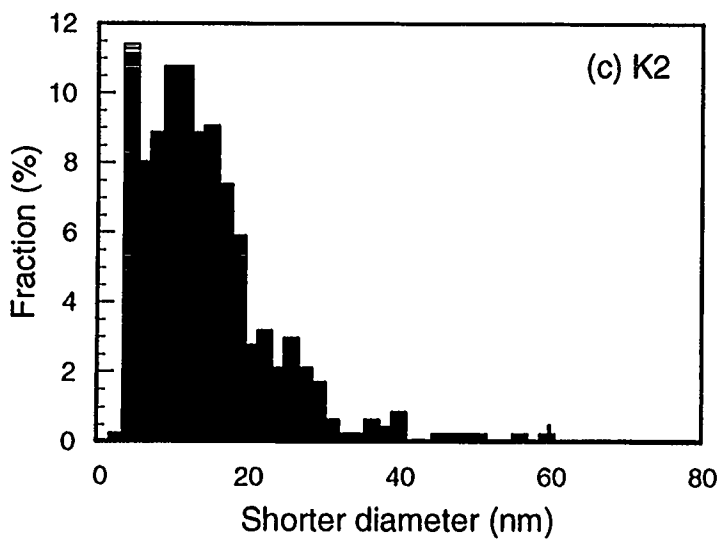

Figure 5 Diametral size distributions of pores in unirradiated (a) K1, (b) K3 and (c) K2.

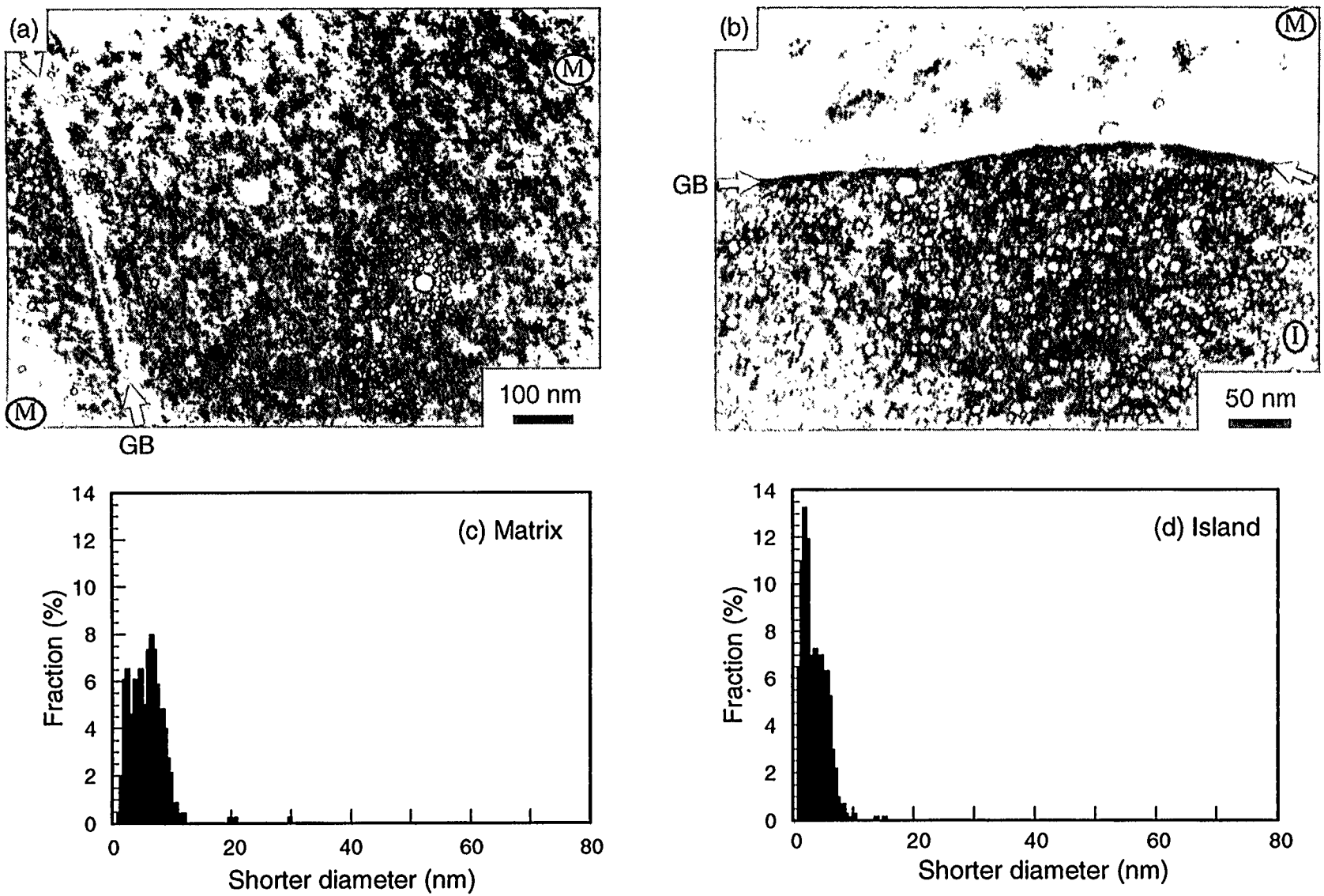

Figure 6 Cavities and diametral size distributions in matrix ((a), (c)) and island ((b), (d)) of irradiated K1.

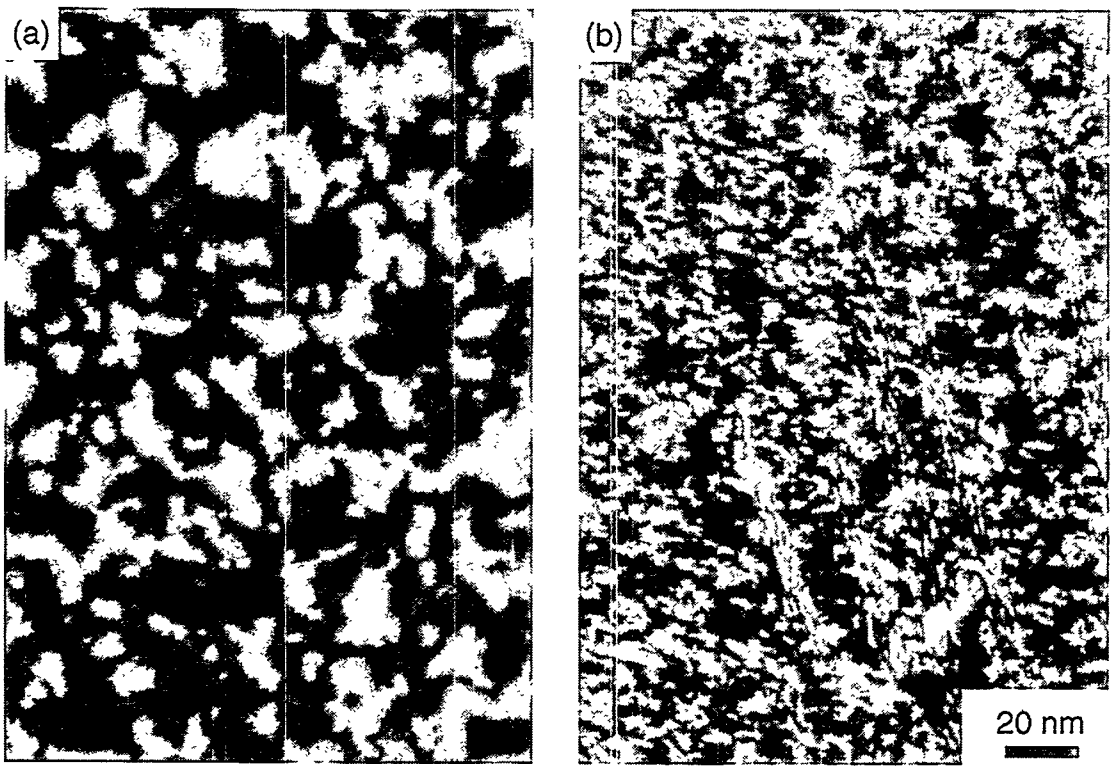

Figure 7 Weak-beam dark-field images in (a) matrix and (b) island of irradiated K1.

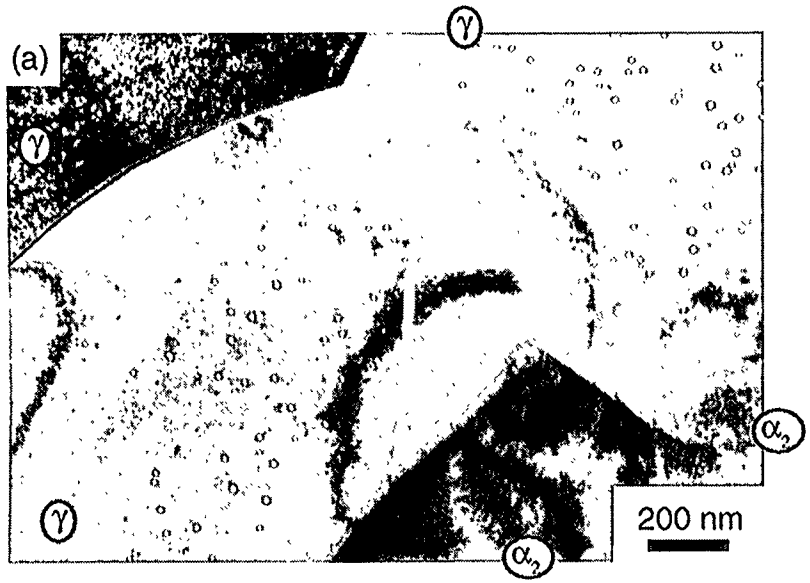

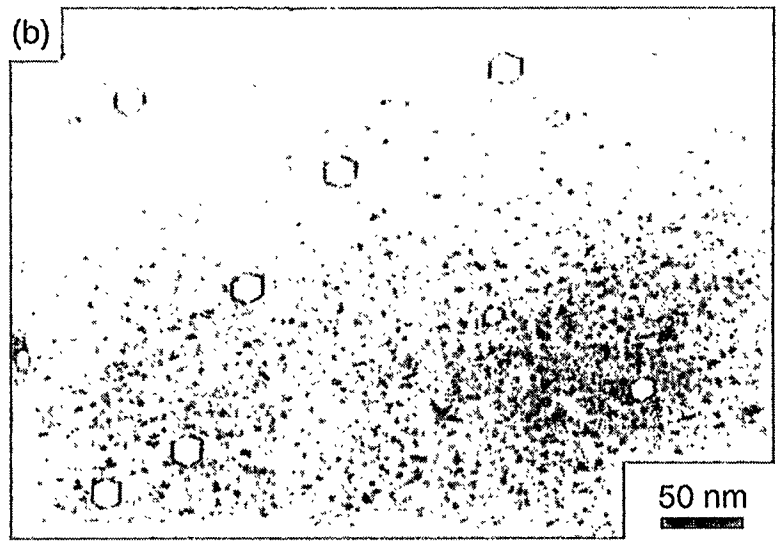

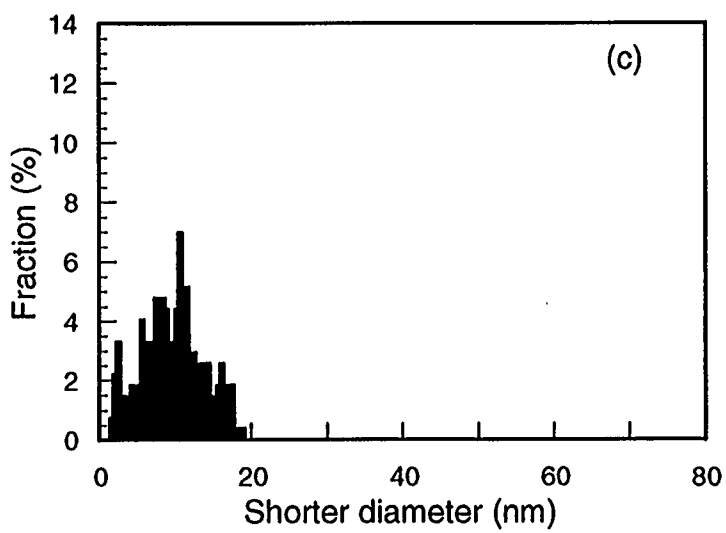

Figure 8 Cavities and diametrall size distribution of cavities in γ-TiAl of irradiated K3.
(a) Cavity free zones along γ-γ and α_2-γ grain boundaries; (b) Cavities in γ grain.

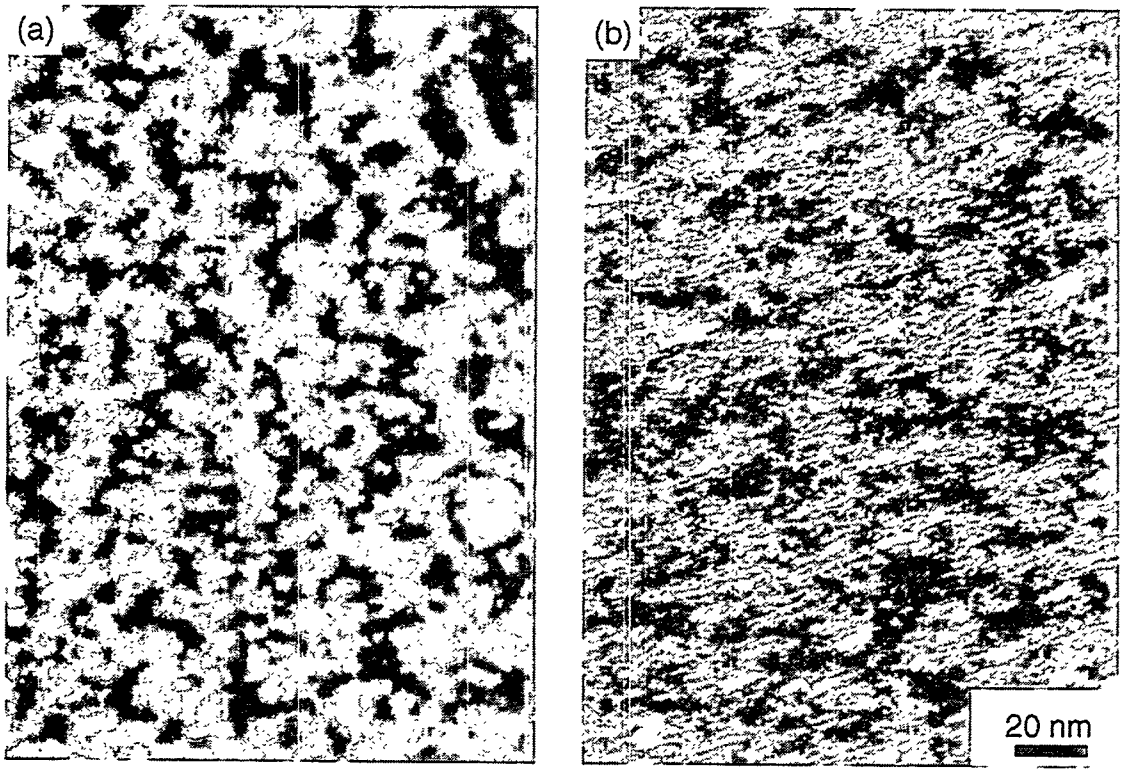

Figure 9 Weak-beam dark-field images in (a) γ-TiAl and (b) α_2-Ti_3Al of irradiated K3.

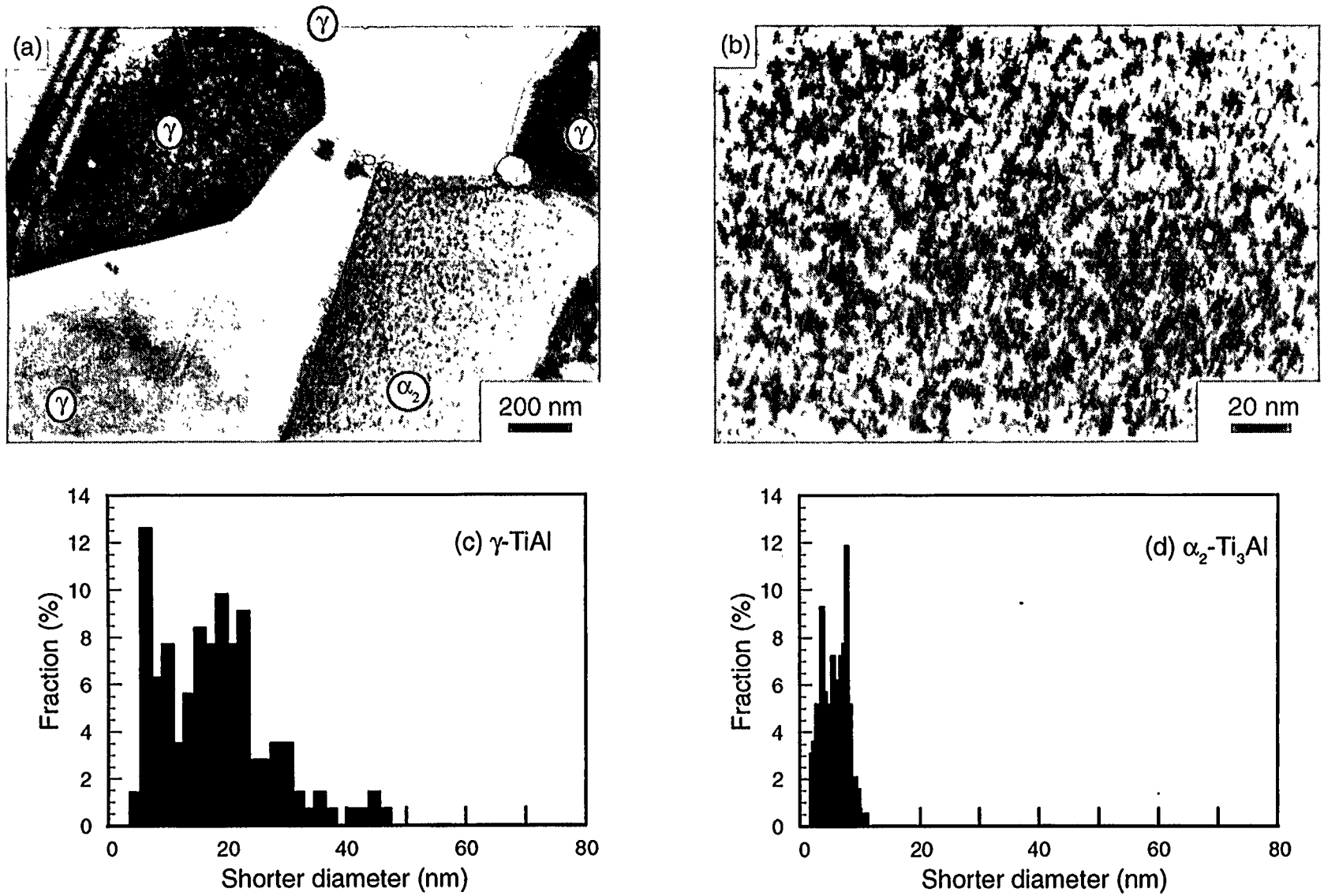

Figure 10 Cavities and diametral size distributions in γ-TiAl ((a), (c)) and α_2-Ti_3Al ((b), (d)) of irradiated K2.

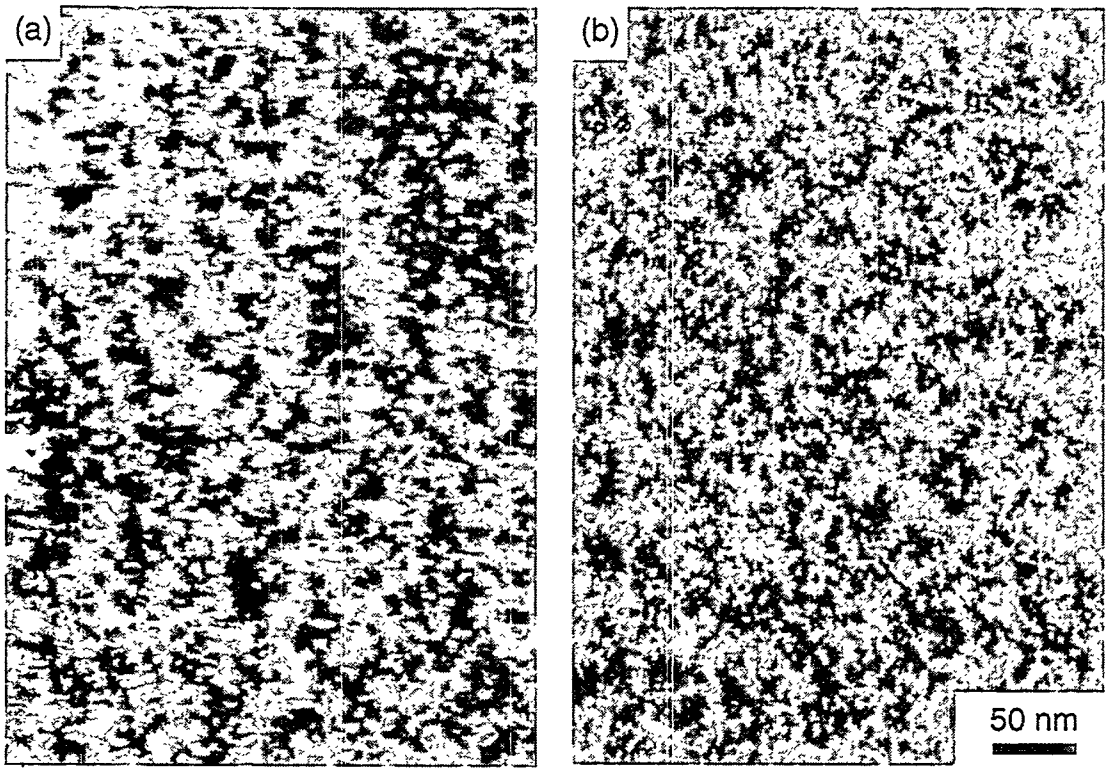

Figure 11 Weak-beam dark-field images in (a) γ-TiAl and (b) α_2-Ti_3Al of irradiated K2.

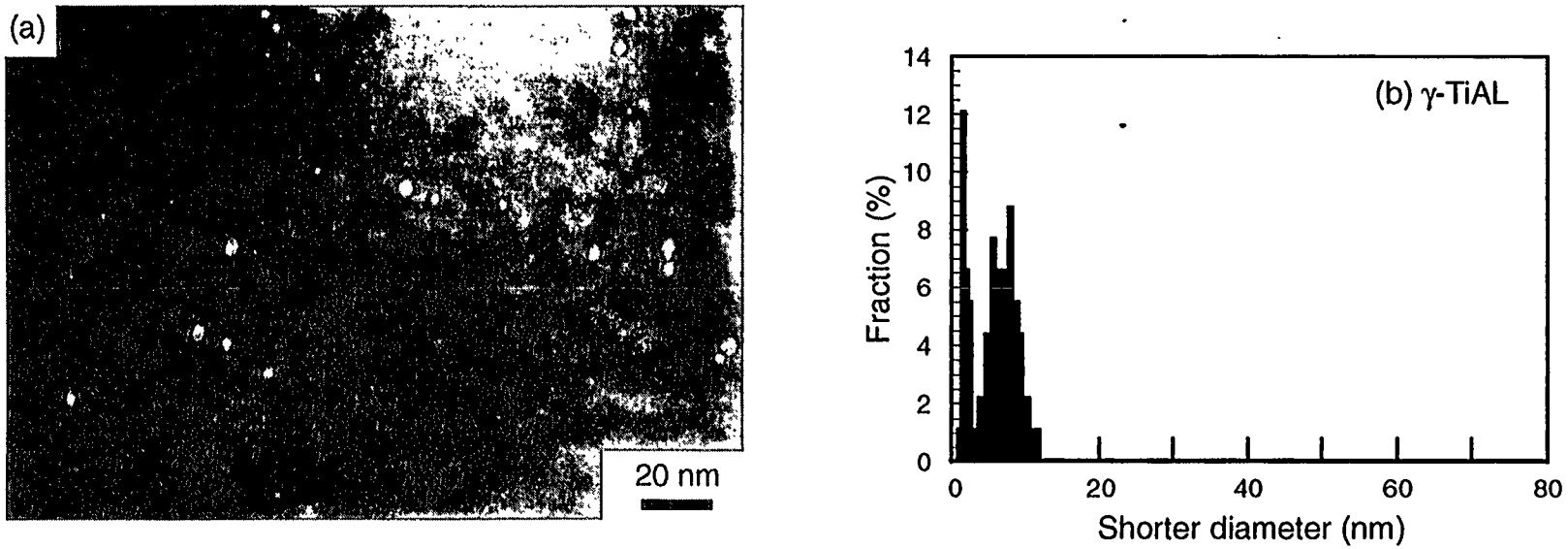

Figure 12 Cavities and diametral size distribution in γ-TiAl of irradiated K4.

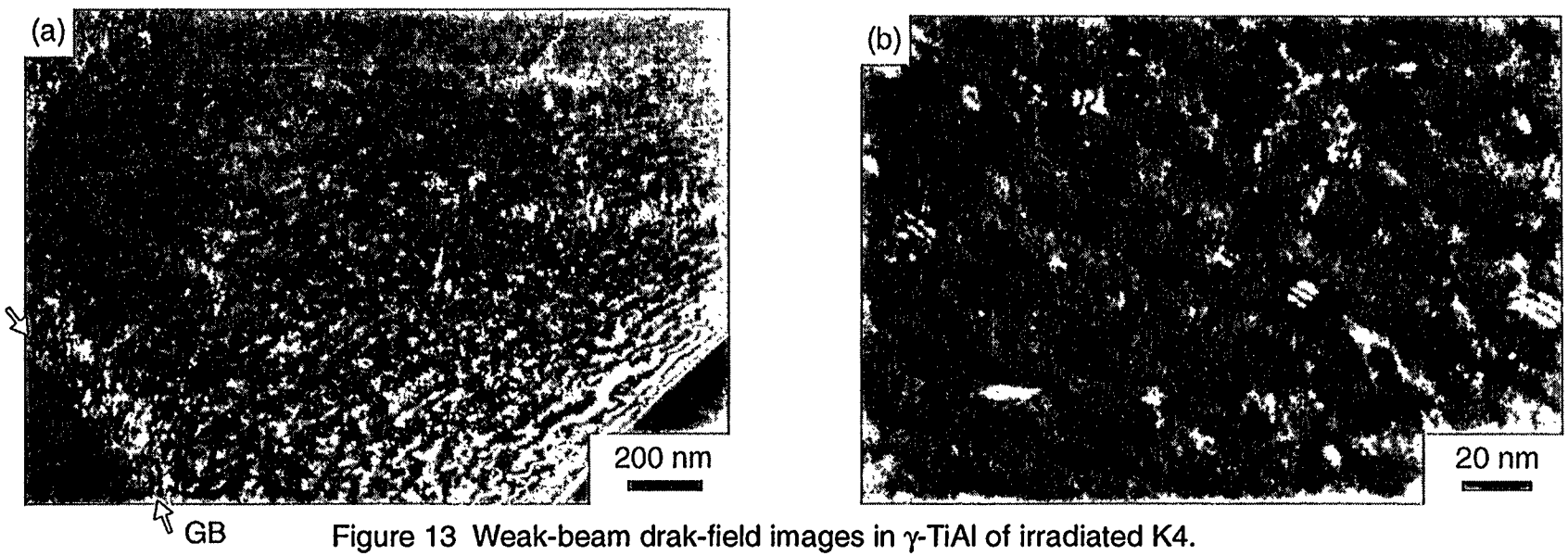

Figure 13 Weak-beam drak-field images in γ-TiAl of irradiated K4.